Magnetoreflectance at the band edge in $Cd_{1-x}Mn_xSe$

R. L. Aggarwal

Francis Bitter National Magnet Laboratory and the Department of Physics, Massachusetts Institute of Technology, Cambridge, Massachusetts 02139

S. N. Jasperson,* J. Stankiewicz,† and Y. Shapira

Francis Bitter National Magnet Laboratory, Massachusetts Institute of Technology, Cambridge, Massachusetts 02139

S. Foner

Francis Bitter National Magnet Laboratory and the Department of Physics, Massachusetts Institute of Technology, Cambridge, Massachusetts 02139

B. Khazai and A. Wold

Department of Chemistry, Brown University, Providence, Rhode Island 02912

(Received 1 June 1983; revised manuscript received 12 September 1983)

Magnetoreflectance measurements of excitonic interband transitions are used to study the exchange interaction between band electrons and Mn ions in $Cd_{1-x}Mn_xSe$ ($x = 0.10$ and 0.30) at 1.5 K and over an applied magnetic field range of 0–15 T. By combining optical data with direct magnetization measurements performed on the $x = 0.10$ sample, the difference between the conduction- and valence-band exchange constants, $N_0(\alpha - \beta)$, is found to have a value of 1.37 ± 0.07 eV. Given from previous work that $N_0\alpha = 0.26 \pm 0.01$ eV, a value of -1.11 ± 0.07 eV is obtained for the valence-band exchange constant $N_0\beta$. Additionally, the detailed behavior of the conduction-band and A, B, and C valence-band splittings with applied magnetic field is calculated from theory and shown consistent with measured results. In the case of A excitons, the calculations are in close quantitative agreement with measurements; for B excitons, the agreement is only qualitative.

I. INTRODUCTION

$Cd_{1-x}Mn_xSe$ belongs to the class of II-VI compound semiconductors in which a fraction of the group-II cadmium atoms are replaced by manganese. The assumption is made that all manganese atoms enter substitutionally as Mn^{2+}, thus retaining their free-space magnetic moment which corresponds to spin $\frac{5}{2}$ and arises from the half-filled $3d$ subshell. Such semiconductors, referred to as semimagnetic semiconductors, possess a large exchange interaction between the spin of the band electron and the spin of the magnetic ion. As a result of this large exchange interaction, semimagnetic semiconductors exhibit unique electrical, optical, and magnetic properties which are extremely sensitive to the application of an external magnetic field.[1,2]

Interband magnetoreflection provides a simple method for determining the exchange constants of cubic crystals, as demonstrated by Gaj, Planel, and Fishman[3] in the case of $Cd_{1-x}Mn_xTe$. In this paper, we report magnetoreflectance measurements of excitonic interband transitions in $Cd_{1-x}Mn_xSe$, which is a hexagonal crystal. Because the crystal symmetry is hexagonal, rather than cubic, it is not possible to solve for the individual exchange constants on the basis of magnetoreflectance measurements in the straightforward manner of Ref. 3. However, the exchange constant $N_0\alpha$ for conduction electrons in $Cd_{0.9}Mn_{0.1}Se$ has been previously measured by Shapira, Heiman, and Foner[4] using spin-flip Raman scattering in conjunction with magnetization data. Given their value of 0.26 eV for $N_0\alpha$, we deduce a value of -1.11 eV for the exchange constant $N_0\beta$ for valence electrons, yielding a ratio $\alpha / |\beta| = 0.23$, which is almost a factor of 2 smaller than a previously quoted value[5] of 0.4, but is in agreement with the value of 0.22 obtained by Komarov *et al.*[6]

Experimental details of this work are summarized in Sec. II, followed in Sec. III by the theoretical background necessary for interpreting the optical spectra measured in the case of a hexagonal semimagnetic crystal such as $Cd_{1-x}Mn_xSe$. Experimental results are presented in Sec. IV, along with a discussion of the conclusions drawn from the data analysis.

II. EXPERIMENTAL DETAILS

Single crystals of $Cd_{1-x}Mn_xSe$, $x \neq 0$, used in this work were all grown by modified Bridgman techniques. The $x = 0.10$ sample was grown at Brown University[7]; the $x = 0.30$ sample was obtained from the Instituto Venezolano de Investigaciones Científicas, Venezula. A CdSe ($x = 0$) sample, which was included in the experiment for comparison purposes, was vapor phase grown and obtained commercially.[8] The $x = 0$ sample was oriented with its optical face normal to the c axis. The $x = 0.10$ and 0.30 samples, on the other hand, were available to us in orientations with face normals tilted with respect to the c axis by 23.5° and 8.0°, respectively. The optical faces of all samples were mechanically ground and polished and

then etched for approximately 1 min in a 0.5% mixture of bromine in methanol.

Magnetoreflectance spectra were measured in the Faraday configuration using the following optical components: a Perkin-Elmer single-pass monochromator, model 99G; a Polaroid sheet polarizer, model HNCP, fabricated to produce circularly polarized light at $\lambda = 0.56$ μm (2.21 eV); and an EG&G silicon photodiode, model SGD-444. The monochromator was equipped with an 1800 grooves/mm Bausch & Lomb grating blazed at $\lambda_B = 0.50$ μm, and its slits were adjusted to produce a monochromatic beam of 3 meV full width at half maximum. A Corning glass filter, No. CS3-73, was also mounted at the entrance slit of the monochromator to eliminate all but the first-order diffracted beam. The light beam was chopped at 510 Hz and the photodetector output synchronously measured with a Princeton Applied Research (PARC) lock-in detector, model 5101. $Cd_{1-x}Mn_xSe$ samples with one optically polished face were placed in an immersion Dewar and maintained at a temperature of 1.5 K by pumping the liquid-helium bath. The external magnetic field, provided by a Bitter magnet with a 2-in bore, was normal to the optical face and, because of geometrical considerations in the optical system, the light beam was inclined 6° from normal incidence. A 5° tilt in the orientation of the Dewar windows reduced the intensity of window reflected light in the collected beam below a detectable level. The system transmittance was measured separately with an aluminum mirror put in place of the semimagnetic sample, and the magnetoreflectance spectra of the $Cd_{1-x}Mn_xSe$ samples were obtained as the ratio of pairs of measured spectra, one from the sample and the second from the high reflectance, spectrally featureless mirror. The precision limit of random effects in such spectra was comparable to the width of the line used to graph representative spectra in Sec. IV.

Magnetization measurements were made by means of a vibrating-sample magnetometer[9] on portions of the same samples used in the magnetoreflectance studies. The temperature of the sample during this experiment was the same as that during the optical work, 1.5 K, but the range of the applied magnetic field provided by the superconducting magnet used during this phase of the work was limited to 0—8 T.

III. THEORETICAL BACKGROUND

Theoretical analyses of the band structure near the zone center of wurtzite crystals have been developed by Hopfield,[10] Adler,[11] and others,[12] and extended to include the exchange interaction between band electrons and magnetic ions by Komarov *et al.*[6] and Gubarev.[13] We summarize briefly the aspects of this previous work relevant to the present discussion and show the resulting energy-level scheme appropriate to $Cd_{1-x}Mn_xSe$ in a magnetic field.

We begin by considering the topmost (*P*-like) valence bands, for which electron wave functions can be expressed conveniently in terms of six basis states

$$(X_+, X_-, Z) \otimes (\uparrow, \downarrow) \ ,$$

where

$$X_\pm = \frac{1}{\sqrt{2}}(X \pm iY) \ ,$$

and X, Y, and Z are functions that transform as the atomic wave functions P_x, P_y, and P_z, respectively. The spin states $(\uparrow, \downarrow)$ are, respectively, parallel and antiparallel to the z axis, which itself is assumed collinear with the crystal c axis. An external magnetic field $\vec{\mathscr{B}}$ is oriented at an angle θ relative to the c axis. With respect to this basis set, the valence-band Hamiltonian at $k = 0$ can be written as

$$\mathscr{H} = \begin{bmatrix} \delta\cos\theta & \delta\sin\theta & 0 & 0 & 0 & 0 \\ \delta\sin\theta & -2\Delta_2-\delta\cos\theta & -\sqrt{2}\Delta_3 & 0 & 0 & 0 \\ 0 & -\sqrt{2}\Delta_3 & -\Delta_1-\Delta_2+\delta\cos\theta & 0 & 0 & \delta\sin\theta \\ 0 & 0 & 0 & -\delta\cos\theta & \delta\sin\theta & 0 \\ 0 & 0 & 0 & \delta\sin\theta & -2\Delta_2+\delta\cos\theta & \sqrt{2}\Delta_3 \\ 0 & 0 & \delta\sin\theta & 0 & \sqrt{2}\Delta_3 & -\Delta_1-\Delta_2-\delta\cos\theta \end{bmatrix} \begin{array}{l} (X_+\uparrow) \\ (X_+\downarrow) \\ (Z\uparrow) \\ (X_-\downarrow) \\ (X_-\uparrow) \\ (Z\downarrow) \end{array} \ , \tag{1}$$

where Δ_1 is the crystal-field-splitting constant due to the noncubic crystal field, Δ_2 and Δ_3 are constants of the spin-orbit interaction, and δ is the exchange energy due to the spin-spin interaction between a valence-band electron and the magnetic ions polarized by the external field. The energy of direct interaction between the applied magnetic field and the electron spin is not included, because it is negligible compared to these other energies. The six basis states are shown parenthetically in the column to the right of the $\mathscr{H}$ matrix to make the ordering of the terms in the Hamiltonian evident. In the mean-field approximation, the exchange energy is given by

$$\delta = \tfrac{1}{2}N_0\beta x \langle S \rangle \ , \tag{2}$$

where N_0 is the density of cations, β is the exchange integral, x is the mole fraction of Mn^{2+} ions, and $\langle S \rangle$ is the magnitude of the thermal average of Mn^{2+} spins. $\langle \vec{S} \rangle$ is assumed to be collinear with the applied magnetic field. In the case of $Cd_{1-x}Mn_xSe$, β is found to have a negative value; thus δ is also a negative quantity.

In the special case of the magnetic field parallel to the c axis $(\theta = 0)$, the eigenvalues of this Hamiltonian are readily found to be

$$E_{A,\pm 3/2} = \pm \delta ,$$

$$E_{B,\pm 1/2} = \frac{-(\Delta_1 + 3\Delta_2) + [(\Delta_1 - \Delta_2)^2 + 8\Delta_3^2 + 4\delta^2 \mp 4\delta(\Delta_1 - \Delta_2)]^{1/2}}{2} , \qquad (3)$$

$$E_{C,\pm 1/2} = \frac{-(\Delta_1 + 3\Delta_2) - [(\Delta_1 - \Delta_2)^2 + 8\Delta_3^2 + 4\delta^2 \mp 4\delta(\Delta_1 - \Delta_2)]^{1/2}}{2} ,$$

corresponding to the energy eigenstates

$$|\tfrac{3}{2},\tfrac{3}{2}\rangle = X_+\uparrow, \quad |\tfrac{3}{2},-\tfrac{3}{2}\rangle = X_-\downarrow \quad \text{for the } A \text{ band },$$

$$|\tfrac{3}{2},\tfrac{1}{2}\rangle = C_1 X_+\downarrow - C_2 Z\uparrow, \quad |\tfrac{3}{2},-\tfrac{1}{2}\rangle = C_1 X_-\uparrow + C_2 Z\downarrow \quad \text{for the } B \text{ band }, \qquad (4)$$

$$|\tfrac{1}{2},\tfrac{1}{2}\rangle = C_2 X_+\downarrow + C_1 Z\uparrow, \quad |\tfrac{1}{2},-\tfrac{1}{2}\rangle = C_2 X_-\uparrow - C_1 Z\downarrow \quad \text{for the } C \text{ band }.$$

In the case of a cubic environment ($\Delta_1 = 0$) and in the absence of magnetic ions ($\delta = 0$), the A and B bands are degenerate, and the spin-orbit splitting between A and C bands is found to be $E_A - E_C = 3\Delta_2 = 3\Delta_3$. The presence of the noncubic crystal-field term Δ_1 lifts the degeneracy between the A and B bands, causing an energy splitting $E_A - E_B \simeq \frac{2}{3}\Delta_1$, provided $\Delta_1 \ll \Delta_2$. Finally, the presence of δ lifts the spin degeneracy of all three bands. In the

case of the $m_j = \pm \frac{3}{2}$ levels, the splitting for $\theta = 0$ is proportional to δ; however, the functional dependence in the $m_j = \pm \frac{1}{2}$ cases is much more complicated because of the mixing of spin-$\frac{1}{2}$ basis states by the combined action of the crystal field and magnetic interaction.

In a similar manner, the energies of the S-like conduction-band levels can be written as

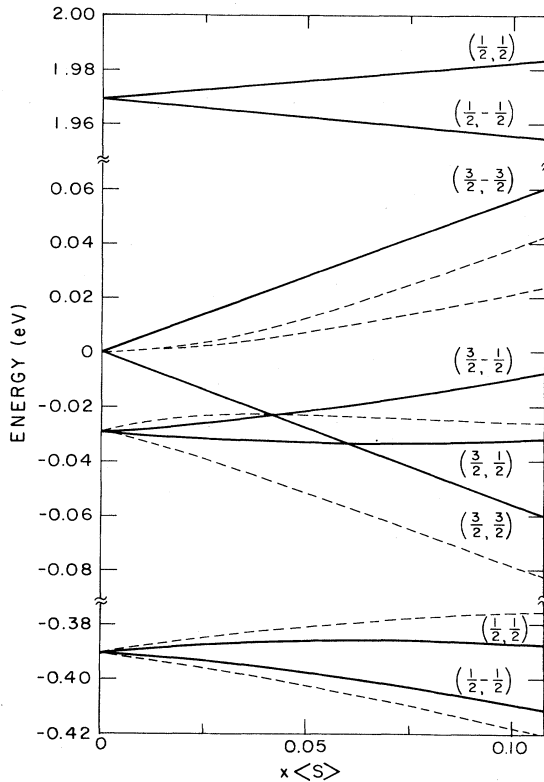$$E_{\text{cond},\pm 1/2} = E_g \pm \tfrac{1}{2} N_0 \alpha x \langle S \rangle , \qquad (5)$$

where α is the value of the conduction-electron—magnetic-ion exchange integral and E_g is the energy of the band gap.

On the basis of the foregoing analysis, an energy-level diagram for $Cd_{1-x}Mn_xSe$ can be constructed, showing conduction-band and A, B, and C valence-band energies plotted versus $x\langle S \rangle$. Figure 1 shows such a diagram in which the $x = 0.10$ experimental results discussed in Sec. IV have been used to determine numerical values for the several energy parameters. These energies are $\Delta_1 = 0.048$ eV, $\Delta_2 = 0.124$ eV, $\Delta_3 = 0.125$ eV, $N_0\alpha = 0.26$ eV, $N_0\beta = -1.11$ eV, and $E_g = 1.969$ eV. Band energies for $\theta = 0°$ are shown as solid curves; for comparison, energies for $\theta = 90°$ are shown as dashed curves. We note in particular the effect of the noncubic crystal field, which lowers the B valence-band energy relative to the A valence band and causes the splitting of the B and C valence bands to be asymmetric.

The excitonic interband transitions studied in this experiment are shown in Fig. 2 as vertical lines connecting the appropriate A or B valence-band and conduction-band levels, all of which are shown split by the action of an applied magnetic field. The polarization of each transition is indicated, with σ^+ and σ^- corresponding to $\Delta m_j = +1$ and -1, respectively. The transitions are also ordered according to energy, which increases from left to right in the figure. This underscores the fact that in the case of B excitons, the theory gives σ^+ energies which are greater than the σ^- energies, a feature found consistent with experiment in the next section. Although the vertical lines in Fig. 2 depict simple interband transitions, in reality they represent the formation of ground-state excitons. No distinction is made because we assume, in subsequent analysis of experimental data, that the binding energy of the exciton (0.016 eV) is independent of the applied magnetic field.

FIG. 1. Diagram of energy levels of the lowest conduction band and the A, B, and C valence bands of $Cd_{0.9}Mn_{0.1}Se$ as a function of magnetization, expressed as $x\langle S \rangle$. Solid curves correspond to the $\theta = 0°$ ($\vec{B} \parallel c$), dashed curves to $\theta = 90°$ ($\vec{B} \perp c$). The (j,m_j) label for each level in the case of $\theta = 0°$ is shown parenthetically. Dashed curves are not similarly labeled because m_j is not a good quantum number for $\theta = 90°$.
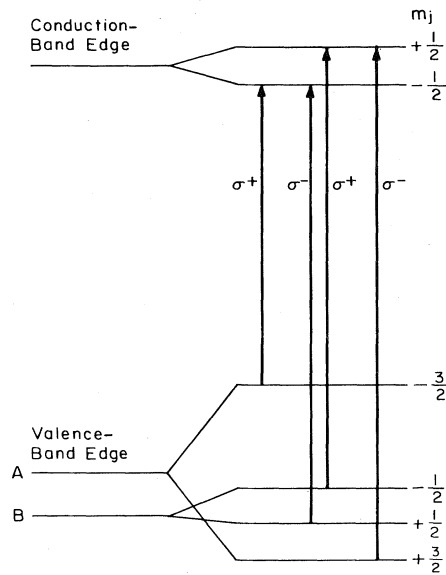
FIG. 2. Schematic diagram of the magnetically split energy bands involved in the excitonic transitions considered in this paper. Optical transitions are indicated by vertical lines connecting the appropriate valence- and conduction-band states. These transition are ordered in energy, energy increasing from left to right, and the polarization is shown, σ^+ corresponding to $\Delta m_j = +1$, σ^- to $\Delta m_j = -1$.

IV. RESULTS AND DISCUSSION

Representative magnetoreflectance spectra are shown in Fig. 3 for applied field strengths of $\mathscr{B} = 0$ and 15.04 T. These spectra show a large splitting with magnetic field of the structure associated with the A exciton, but almost negligible splitting of the B-exciton structure. The resonant energy value of each structure is taken at the midpoint of its negatively sloped portion. Optical polarizations of the two high-field spectra are labeled σ^+ and σ^- in accordance with the convention given in the preceding section.

In order to examine the correlation between the optical splittings and the Mn^{2+} spin alignment, measurements of the magnetization of the $x = 0.10$ and 0.30 samples were also made. These data are shown in Fig. 4 as $x\langle S \rangle$ versus applied field. Note that for $x = 0.10$ the magnetization does not vary appreciably in fields above ~ 6 T. In contrast, the magnetization for $x = 0.30$ is strongly field dependent even above 6 T.

In the manner suggested in Ref. 3, magnetization data were fitted by a least-squares procedure to the empirical relation

$$\langle S \rangle = S_0 B_{5/2}(5\mu_B \mathscr{B}/k_B(T+T_0)) , \qquad (6)$$

where $B_{5/2}$ is a Brillouin function of index $\frac{5}{2}$, S_0 is the saturation spin value, μ_B is the Bohr magneton, k_B is the Boltzmann constant, $T = 1.5$ K, and T_0 is an adjustable temperature parameter. The best fit for $x = 0.10$ data gives $S_0 = 0.97$ and $T_0 = 2.29 \pm 0.02$ K. This fit is plotted
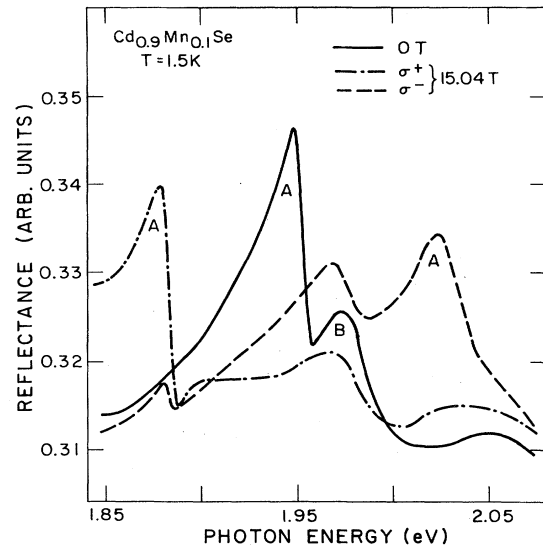

FIG. 3. Magnetoreflectance spectra for $Cd_{0.9}Mn_{0.1}Se$ at a temperature of 1.5 K in applied magnetic fields of 0 and 15.04 T. The excitonic structures appearing in these spectra are labeled with the appropriate valence band and polarization states, consistent with the convention given in Fig. 2.

as a solid line in Fig. 4 and illustrates the fact that Eq. (6) describes the magnetization behavior quite closely, at least in the 0—8 T range for an $x = 0.10$ sample. The value of S_0 obtained above is 39% of the maximum possible value
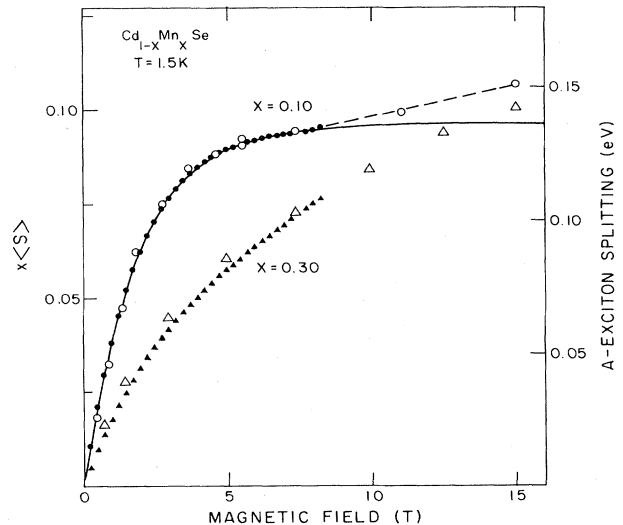

FIG. 4. Magnetization and optical data for the $x = 0.10$ (circles) and $x = 0.30$ (triangles) samples plotted as a function of the external magnetic field. Solid circles and triangles indicate magnetization data, expressed as $x\langle S \rangle = \frac{5}{2}(M/M_0)x$, where M_0 is the maximum theoretical value of the magnetization for a given concentration. For $x = 0.10$, $M_0 = 15.0$ emu/g; for $x = 0.30$, $M_0 = 48.1$ emu/g. Open circles and triangles indicate the energy splitting of the A exciton. The solid curve is a least-squares fit of a Brillouin function to the $x = 0.10$ magnetization data. The dashed line simply provides a visual connnection between adjacent optical data points for $x = 0.10$ in the high-field region.
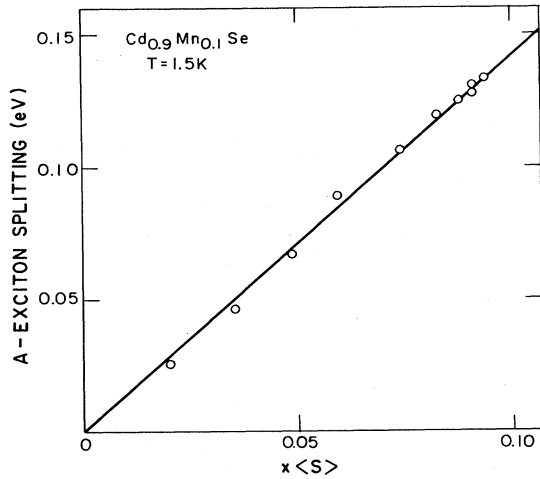
FIG. 5. Energy splitting between σ^+ and σ^- transitions of A exciton versus magnetization, expressed as $x \langle S \rangle$. The solid line is a straight line of slope 1.41 eV, adjusted to best fit the data.

$(\frac{5}{2})$ and corresponds to a magnetization of 5.84 ± 0.01 emu/g. It is noteworthy that these results are in good agreement with the magnetization data measured in an earlier experiment with an $x = 0.106$ sample obtained from another source.[4] In the case of $x = 0.30$, however, no best fit is shown because the $\mathcal{B}$ dependence of $\langle S \rangle$ cannot be well represented by a Brillouin function.

A exciton optical splitting data are also plotted in Fig. 4, with the energy axis scaled for the best fit between optical and magnetization data obtained with the $x = 0.10$ samples in the range 0–8 T where the two sets of measurements overlap. In the case of $x = 0.10$, the resulting correspondence between the two data sets appears quite good. However, the optical splittings at 11 and 15 T are higher than the extrapolated values obtained from the Brillouin-type behavior below 8 T. A dashed line through the last three high-field optical data points is included in Fig. 4 to approximate the behavior of the optical splitting, and presumably of the magnetization also, in the 8–15 T region. In the case of $x = 0.30$, the optical data points have been plotted using the $x = 0.10$ scale factor. We note that the optical and magnetization measurements for $x = 0.30$ exhibit the same overall trend, although the correspondence could be improved by a small adjustment of the scale factor.

A more useful way to display the correspondence between optical and magnetization data is to eliminate $\mathcal{B}$ as a variable and to plot A exciton splitting versus magnetization directly. As noted in Ref. 3 [see also our Eqs. (2), (3), and (5)], the slope of this graph for the case $\theta = 0$ is proportional to the difference between the values of the conduction- and valence-band exchange integrals:

$$\Delta E = N_0(\alpha - \beta)x \langle S \rangle ,$$ (7)

where ΔE is the splitting between the σ^+ and σ^- A excitons. Even for $\theta \lesssim 23.5°$, it turns out that the proportionality constant between ΔE and $x \langle S \rangle$ is approximately equal to $N_0(\alpha - \beta)$, as we have found in the case of the

$x = 0.10$ sample for which $\theta = 23.5°$.

Figure 5 shows ΔE vs $x \langle S \rangle$ for the $x = 0.10$ sample. A best-fit straight line of slope 1.41 eV is included to show the linear relationship between the two quantities. By solving for the energy eigenvalues in Eq. (1) for both $\theta = 0°$ and 23.5° and for appropriate values of δ, one finds that ΔE is somewhat higher for $\theta = 23.5°$ than for $\theta = 0°$ over most of the $\mathcal{B}$ field range. Correcting for the effect of a finite θ on ΔE, point by point, we obtain in the case of the $x = 0.10$ sample (in eV)

$$N_0(\alpha - \beta) = 1.37 \pm 0.07 .$$ (8)

The uncertainty in this quantity is due almost entirely to the 5% absolute uncertainty in the magnetization measurements.

A similar analysis of the four ΔE measurements between 0 and 8 T for the $x = 0.30$ sample yields a value of 1.48 eV for $N_0(\alpha - \beta)$, which is somewhat outside the uncertainty limits of the $x = 0.10$ value quoted above. We have chosen to state this result separately rather than to combine the two results because spectra for the $x = 0.10$ sample are better resolved than those for the $x = 0.30$ sample.

Inasmuch as Shapira, Heiman, and Foner[4] have independently obtained a value for the conduction-band exchange constant, $N_0\alpha = 0.261 \pm 0.013$ eV, we can use Eq. (8) to evaluate the A band exchange constant, namely,

$$N_0\beta = 0.26 - 1.37 = -1.11 \pm 0.07$$ (9)

in eV. This yields the ratio $\alpha / |\beta| = 0.23 \pm 0.02$, in agreement with the value of 0.22 reported by Komarov et al.[6] The origin of all the energy parameters used in plotting the band energies versus magnetization in Fig. 1 can now be summarized: Δ_1, Δ_2, and Δ_3 were obtained as a set of energies consistent with $E_A - E_C = 0.390$ eV obtained from published electroreflectance data[14] and $E_A - E_B = 0.029$ eV from zero-field data shown in Fig. 3; $N_0\alpha$ was obtained from published literature,[4] $N_0\beta$ was obtained as described above; and E_g was obtained by adding the 16-meV A exciton binding energy[15] to the zero-field ground-state A exciton transition energy shown in Fig. 3.

Given these energy parameters and the magnetization versus applied magnetic field measurements of Fig. 4, it is a straightforward matter to calculate optical transition energies versus $\mathcal{B}$ in order to examine the overall correspondence between the optical measurements and the predictions of theory. Figure 6 shows such a comparison in the case of the $x = 0.10$ sample. Open (solid) circles locate σ^- (σ^+) excitonic transitions recorded with circularly polarized light, and triangles locate transitions recorded in one experiment with unpolarized light. The solid lines depict transition energies between levels, evaluated from Eqs. (1) and (5) with $\theta = 23.5°$. A small, positive quadratic offset of $3\mathcal{B}^2/(15)^2$ meV T^{-2} was added to the transition energies in all four branches in order to take into account a diamagnetic shift observed in spectra obtained from the $x = 0$ sample. Values for $x \langle S \rangle$ vs $\mathcal{B}$ in the range 8–15 T were calculated in a self-consistent fashion from Eqs. (7) and (9), using ΔE measurements corrected to $\theta = 0°$. The vertical placement of the calculated curves was adjusted for the best fit with the A exciton data. The rms residual
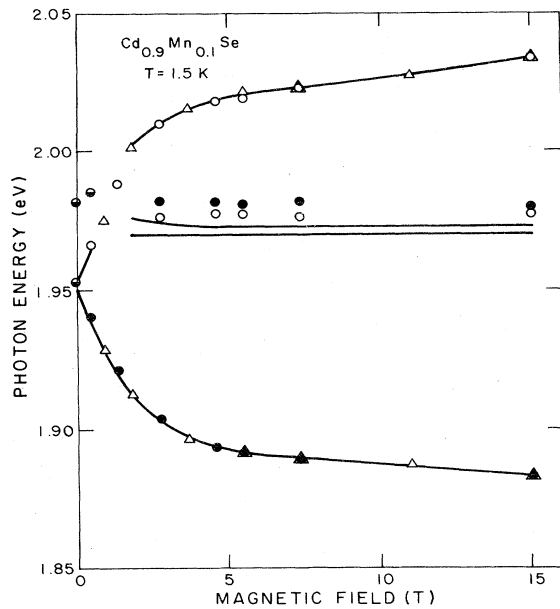
FIG. 6. Comparison of measured A and B exciton transition energies (circles and triangles) with those calculated from Eqs. (1) and (5) (solid lines) for the $x = 0.10$ sample, $\theta = 23.5°$. Solid circles indicate σ^+ transitions, open circles indicate σ^-, and the triangles locate data points obtained in an experiment using unpolarized light.

scatter between corresponding measured and calculated A exciton energies is found to be less than 0.001 eV. Calculated values are not shown for the B-exciton and the σ^- A-exciton energies in the level crossing region between 0.5 and 1.8 T because of complications arising from the interaction between A and B bands when $\theta \neq 0$.

Several useful observations and inferences can be made upon examination of Fig. 6. For instance, the excellent agreement between A exciton measurements and calculations throughout the (0—15)-T range demonstrates the high systematic precision of individual measurements made with this technique. Furthermore, the precision of the calculated value of $N_0(\alpha - \beta)$ can be estimated by examining changes in ΔE vs $\mathscr{B}$ as a result of a fractional change in $N_0(\alpha - \beta)$. A fractional change of $\pm 3\%$, for example, would change ΔE by ± 0.003 eV over most of the field range and noticeably degrade the fit. Also, the fact that extrapolated A exciton calculations in the range 8—15 T fit the data as well as the 0—8 T portions based on direct magnetization measurements further substantiate the linear relationship between ΔE and $x\langle S \rangle$ throughout the applied field range.

In contrast to the A exciton transitions which were adjusted to best fit the experimental data, no separate adjustments were made to affect the relative position of the B exciton transitions. In fact, the only input to the calculations directly involving the B band is the separation ener-

gy between the A and B bands, $E_A - E_B$, measured in Fig. 3. It is thus of interest to examine the correspondence between the calculated predictions of B exciton energies and the measured results, shown also in Fig. 6. We see that the predictions and results follow the same trend of very little change in energy with changing applied field, although there is a substantial average offset of 0.008 eV between them. Another correspondence between the data and the calculated curves is the energy ordering of the σ^+ and σ^- branches. This is significant because the predicted energy ordering of the transitions is a peculiarity of the asymmetric splitting of the B band levels. If, for example, the crystal-field splitting were turned off, the fact that $|\beta/3| > \alpha$ would cause the σ^- transition to move to an energy greater than that of the σ^+. Thus the observed energy ordering indicates that the effect of the crystal field on the B band sublevel splitting is in accord with the predictions of theory.

One unexplained discrepancy between B exciton measurements and published data is the relatively large value for the zero-field splitting $E_A - E_B = 0.029$ eV for this $x = 0.10$ sample. For the $x = 0$ sample, we obtained a splitting of $E_A - E_B = 0.027$ eV, consistent with published values which range from 0.025 to 0.027 eV.[14,15] Moreover, the splitting in the case of $x = 0.30$ was indeed less than 0.027 eV, following the general trend reported by Stankiewicz[14] in which $E_A - E_B$ decreases linearly with increasing x. On this basis, we would expect a splitting of $E_A - E_B = 0.025$ eV, but even the most generous estimates of systematic error in our measurement of $E_A - E_B$ will not justify a value less than 0.027 eV. Whatever the origin of this large value for zero field $E_A - E_B$, B exciton energies at all applied fields are similarly elevated.

Although some questions remain regarding the precise details of the correspondence between data and calculations for B excitons, the qualitative fit is successful in terms of the functional trend of transition energies versus applied field and of the energy ordering of the two B-exciton transitions. Furthermore, the unresolved discrepancies in the case of the B exciton have no bearing on the confidence level of the value of the exchange constant, $N_0\beta$, as deduced from A exciton and magnetization measurements.

ACKNOWLEDGMENTS

*On sabbatical leave from the Department of Physics, Worcester Polytechnic Institute, Worcester, MA 01609.

†Visiting scientist from Centro de Fisica, Instituto Venezolano de Investigaciones Científicas, Caracas 1010A, Venezuela.

[1]J. A. Gaj, in Proceedings of the 15th International Conference on the Physics of Semiconductors, Kyoto, Japan, 1980 [J. Phys. Soc. Jpn. 49, Suppl. A, 797 (1980)].

[2]J. K. Furdyna, J. Appl. Phys. 53, 7637 (1982).

[3]J. A. Gaj, R. Planel, and G. Fishman, Solid State Commun. 29, 435 (1979).

[4]Y. Shapira, D. Heiman, and S. Foner, Solid State Commun. 44, 1243 (1982). See also T. Dietl and J. Spalek, Phys. Rev. Lett. 48, 355 (1982).

[5]M. Nawrocki and R. R. Galazka, as cited in Proceedings of the 15th International Conference on the Physics of Semiconductors, Ref. 1, p. 802.

[6]A. V. Komarov, S. M. Ryabchenko, Yu.G. Semenov, B. D. Shanina, and N. I. Vitrikhovskii, Zh. Eksp. Teor. Fiz. 79, 1554 (1980) [Sov. Phys.—JETP 52, 783 (1980)].

[7]Details of the growth techniques can be found in the article by B. Khazai, R. Kershaw, K. Dwight, and A. Wold. Mater. Res. Bull. 18, 217 (1983).

[8]Eagle-Picher Industries, Inc., Miami, OK.

[9]S. Foner, Rev. Sci. Instrum. 30, 548 (1959).

[10]J. J. Hopfield, J. Phys. Chem. Solids 15, 97 (1960).

[11]S. L. Adler, Phys. Rev. 126, 118 (1962).

[12]G. E. Pikus, Zh. Eksp. Teor. Fiz. 41, 1507 (1961) [Sov. Phys.—JETP 14, 1075 (1962)]; E. Gutsche and E. Jahne, Phys. Status Solidi 19, 823 (1967).

[13]S. I. Gubarev, Zh. Eksp. Teor. Fiz. 80, 1174 (1981) [Sov. Phys.—JETP 53, 601 (1981)].

[14]J. Stankiewicz, Phys. Rev. B 27, 3631 (1983).

[15]See B. Segall and D. T. F. Marple, in Physics and Chemistry of II-VI Compounds, edited by M. Aven and J. S. Prenen (North-Holland, Amsterdam, 1967), Tables 7.3 and 7.4, pp. 343 and 344.